Engineering antiparallel charge-transfer cascades into supramolecular n/p-heterojunction photosystems: Toward directional self-sorting on surfaces

Marco Lista, Jetsuda Areephong, Edvinas Orentas, Pierre Charbonnaz, Naomi Sakai and Stefan Matile*

Received 19th April 2011, Accepted 12th May 2011
DOI: 10.1039/c1fd00072a

This contribution describes recent progress made with the design, synthesis and evaluation of supramolecular architectures for artificial photosynthesis. Emphasis is on the possible introduction of antiparallel redox gradients into the co-axial hole- and electron-transporting channels of supramolecular n/p-heterojunctions, and on directional, uniform axial and alternate lateral self-sorting to get there. Recent results suggest that two-component gradients in both channels are sufficient for photoinduced charge separation over very long distances. Removal of one gradient leads to charge recombination at the usual critical distances, inversion of both gradients causes photocurrent inhibition. These promising results call for user-friendly, cheap and fast approaches to oriented multicomponent architectures on solid surfaces. However, the reduction of efforts devoted to covalent organic synthesis will have to be compensated by the development of strategic concepts on the supramolecular level to tackle basic questions such as self-sorting on surfaces.

Introduction

An important objective with artificial photosynthesis is to apply lessons from nature to organic solar cells.[1] The interaction of matter with light produces in both systems electrons in the excited state and holes left behind in the ground state. To harness the photonic energy, these charges have to be separated and collected before they recombine and everything is lost. Initially, organic solar cells had a bilayer architecture, where a bulk layer of electron-transporting or n-type semiconducting material was covered with a bulk layer of hole-transporting or p-type semiconducting material (Fig. 1a).[2] Bilayer organic solar cells excel with high charge mobility in the individual layers, whereas photoinduced charge separation is less convincing because the contact area between the two layers is very small from a molecular point of view. To increase this interface, bulk n/p-heterojunction solar cells (BHJ) have been introduced (Fig. 1b). In BHJ architectures, n-type and p-type materials are mixed up in many different, often very elegant ways. (Dye-sensitized solar cells successfully use the inorganic chemistry of mesoporous oxide materials for the same purpose).[3] Improved charge separation at the increased n/p-contact area of BHJ photosystems usually comes at the cost of reduced charge mobility in the less ordered, discontinuous n- and p-type materials.

Department of Organic Chemistry, University of Geneva, Geneva, Switzerland. Web: www.unige.ch/sciences/chiorg/matile/; E-mail: stefan.matile@unige.ch; Fax: +41 22 379 5123; Tel: +41 22 379 6523

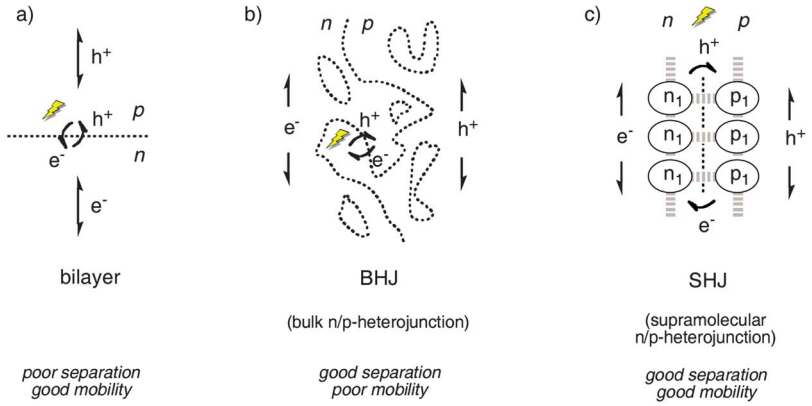

Fig. 1 Schematic architectures of (a) bilayer organic solar cells, (b) BHJ and (c) SHJ photosystems. Efficiency is influenced by photoinduced charge separation at the n/p-contact area (dashed lines) as well as the mobility of holes and electrons in p- and n-type (a) bulk layers, (b) macrodomains or (c) co-axial molecular channels.

To combine the advantages of bilayer and BHJ solar cells without suffering from their complementary shortcomings, supramolecular n/p-heterojunction (SHJ) architectures have been proposed (Fig. 1c).[4–6] In SHJs, hole- and electron-transporting pathways are aligned on the molecular level next to each other. In principle, co-axial and bicontinuous n- and p-channels offer an n/p-contact area that is maximized as far as it possible, down to the molecular level, to maximize photoinduced charge separation, whereas charge mobilities remain high.

The construction of SHJ photosystems has proven difficult despite much effort in many groups. There are several reasons why the SHJ photosystems are slow to live up to their promise, including significant challenges in organic synthesis and supramolecular chemistry. Moreover, whereas the transport of holes and electrons in the molecular n- and p-channels in biological photosystems is directional (Fig. 2a), SHJ architectures operate by passive charge diffusion along their corresponding molecular channels. In the following, we would like to discuss the possibility to engineer oriented multicomponent antiparallel redox gradients (OMARGs) into SHJ photosystems (Fig. 2b).[7,8] The discussion covers conceptual considerations and preliminary results from the first minimalist OMARG-SHJ. The main conclusion is that easier synthetic access to oriented and ordered multicomponent architectures is needed to fully assess the potential of OMARG-SHJ and related photosystems. The development of strategies for directional self-sorting on surfaces—something like 3D Tetris with remote control—is considered as a most promising approach to tackle this challenge.

The following discussion is highly simplified and applies an organic and supramolecular chemistry perspective. Emphasis is on conceptual innovation on a fundamental level that has nothing to do with solar cell engineering and does not aim to increase device efficiencies, at least not at this stage.

The OMARG-SHJ concept

In biological photosystems, photoinduced charge separation occurs in the special pair of chlorophylls.[1,7] Excitation of one of the two chlorophylls (n_1, Fig. 2a) is presumably followed by transfer of the electron to the other chlorophyll (n_2, Fig. 2a). In principle, this ultrafast symmetry-breaking charge separation affords one oxidized chlorophyll radical cation n_1 and one reduced chlorophyll radical anion n_2. To avoid the loss of all photonic energy by immediate charge recombination in the special pair, the electron in the reduced chlorophyll n_2 is then directed along

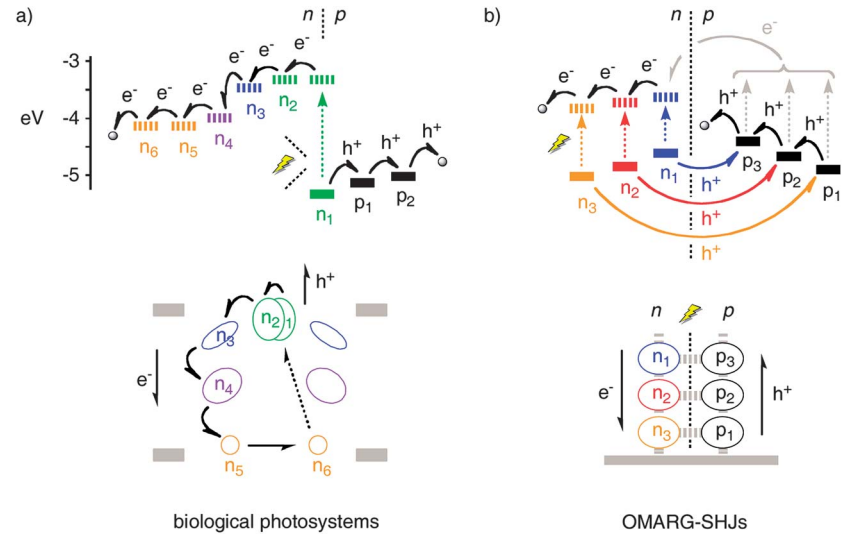

Fig. 2 Energy diagrams (top; solid, HOMO; dashed, LUMO) and schematic architectures (bottom) of redox gradients in (a) biological photosystems and (b) OMARG-SHJs. Everywhere in OMARG-SHJs, excitation of n_x-transporters can be followed by charge separation at the molecular-level n/p-interface (here hole injection into p-channels) and electron and hole transfer along antiparallel redox gradients in the n- and p-channels toward their final destination; excitation of p-transporters followed by electron or energy transfer to the n-channel leads to the same situation (grey).

a multicomponent redox gradient in a molecular-level n-transporting pathway to the ubiquinone QB (n_6, Fig. 2a). The hole left behind in the oxidized chlorophyll n_1 is at the same time moved in the opposite direction along a molecular hole-transporting pathway with a multicomponent redox gradient (p_1, p_2, Fig. 2a).

In summary, the molecular charge-transporting pathways in biological photosystems are equipped with multicomponent redox gradients to direct charges after photoinduced charge separation in opposite directions to never meet again and recombine. The essentials to engineer the corresponding charge-transfer (CT) cascades into the molecular n- and p-channels of SHJs are outlined in Fig. 2b. The programmed assembly of n-transporters n_1, n_2, n_3, *etc.*, with rising LUMO levels at increasing distance from the surface will generate an electron-transfer (ET) cascade in the n-channel that points toward the solid surface. The programmed assembly of p-transporters p_1, p_2, p_3, *etc.*, with rising HOMO levels at increasing distance from the surface will generate an antiparallel redox gradient in the p-channel directing holes toward the surface of the photosystem. The HOMO level of the p-transporter should be higher than that of the coupled n-transporter to allow hole injection into the p-channels at any point in the photosystem. Besides these three main prerequisites, several other considerations deserve attention. For instance, decreasing bandgaps with rising LUMO levels in the n-channel appears important to avoid high-energy traps. High LUMOs (*i.e.*, high bandgaps) in the p-channel appear desirable to block competing electron transport and assure electron injection into the n-channel at any point of the system. The gradients shouldn't be too steep and the bandgaps shouldn't be too small to preserve significant open-circuit voltages at maximized short circuit currents and fill factors.

The construction of multicomponent architectures that fulfil all these requirements is a formidable challenge with regard to synthetic organic and supramolecular chemistry. Whereas general, user-friendly access to functional SHJ photosystems still remains to be refined,[4–6] OMARG-SHJs appear intractable in a general

manner.[7] In the following, recent results from this group in designing and synthesizing the simplest possible OMARG-SHJ, a [2 + 2] OMARG-SHJ with minimalist two-component gradients in both channels,[8] will be described and discussed.

Design and synthesis of [2 + 2] OMARG-SHJs

The multichromophoric donor–acceptor hybrids **1–5** have been designed and synthesized to build the first formal OMARG-SHJ (Fig. 3).[8,9] The so-called initiator **1** contains a short *p*-oligophenyl (POP) scaffold. The POP scaffold is decorated with naphthalenediimides (NDIs) without substituents in the core. Amides and carboxylates in the NDI sidechains are placed for structural reasons only. With regard to function, non-substituted NDIs can serve as electron acceptors and n-type transporters (n_3 in Fig. 4a), whereas POP scaffolds prefer to transport holes (p_1 in Fig. 4a).

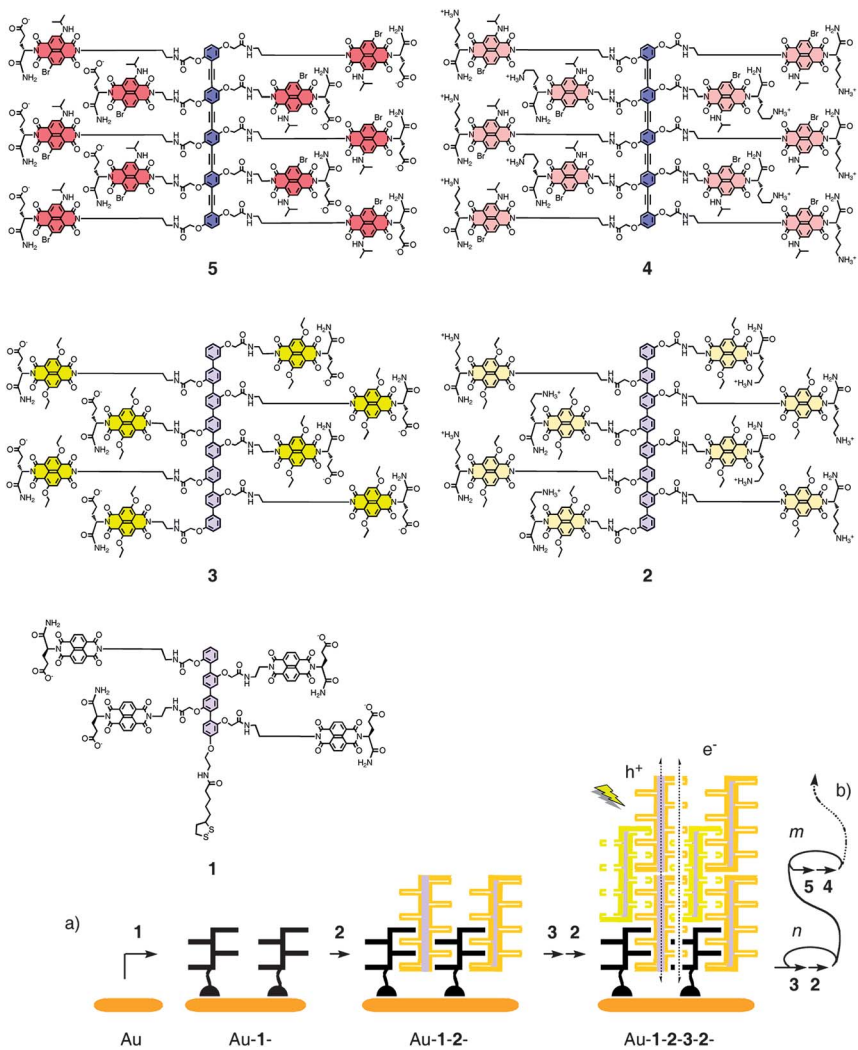

Fig. 3 Structure of molecules synthesized to build [2 + 2] OMARG-SHJs and (a) their zipper assembly on gold surfaces. (b) Efforts to zip up a third domain to build [3 + 3] OMARG-SHJs are ongoing.

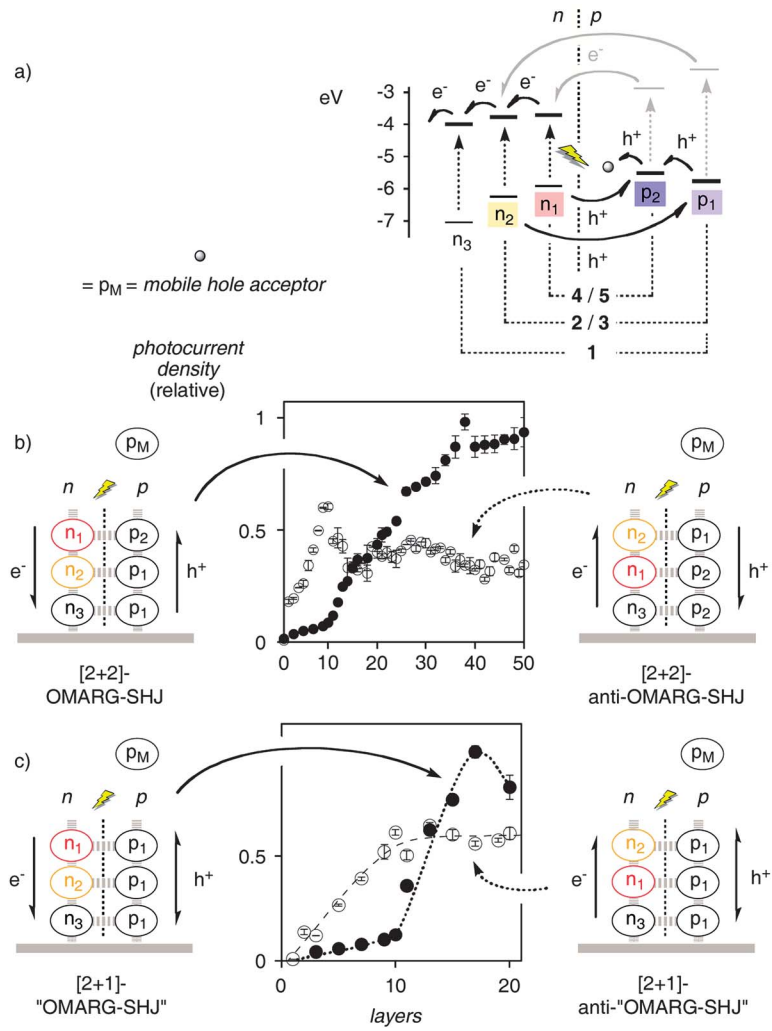

Fig. 4 (a) HOMO/LUMO levels for [2 + 2] OMARG-SHJ Au-**1**-(**2**-**3**-)$_m$-(**4**-**5**-)$_n$- with indication of photoinduced (dashed arrows) e^- (grey) and h^+ injection (black) into the molecular n- and p-channels (bold). b) *J*–*L* profile for [2 + 2] OMARG-SHJ Au-**1**-(**2**-**3**-)$_4$-**2**-(**5**-**4**-)$_n$- (●), and anti-OMARG-SHJ Au-**1**′-(**4**-**5**-)$_4$-**4**-(**3**-**2**-)$_n$- (○). c) *J*–*L* profile for single-gradient [2 + 1] "OMARG-SHJ" Au-**1**-(**2**-**3**-)$_4$-**2**-(**5**′-**4**′-)$_n$- (●), and [2 + 1] anti-"OMARG-SHJ" Au-**1**′-(**4**′-**5**′-)$_4$-**4**′-(**3**-**2**-)$_n$- (○). **1**′ is an initiator with OPE scaffold and red NDIs, **4**′ and **5**′ are propagators with POP scaffold and red NDIs.[8] Data are reproduced with permission from ref. 8. Copyright 2010 American Chemical Society.

The so-called yellow propagators **2** and **3** are designed to assemble yellow SHJ domains. They both are built from a POP scaffold of double length. Yellow NDIs are attached along the scaffold, together with positive and negative charges for **2** and **3**, respectively. NDIs turn yellow with two alkoxy groups in the core. This decreasing bandgap coincides with increasing HOMO and LUMO levels (n_2 in Fig. 4a).

The red propagators **4** and **5**, finally, are conceived to construct red SHJ domains on top of yellow domains. They both contain OPE scaffolds in place of the POP scaffolds in the yellow domain. Hole-transporters like POPs, the HOMO of OPEs is clearly higher (p_2 in Fig. 4a). In both propagators, red NDIs are attached along

the OPE scaffold. Red NDIs are obtained here with one alkylamino and one bromo substituent in the core. The decreasing bandgap coincides with further increasing HOMO and LUMO levels (n_1 in Fig. 4a).

Assembled on top of each other, the n-type NDI π-stacks should contain a red-to-yellow-to-colorless $n_1 \rightarrow n_2 \rightarrow n_3$ gradient that directs electrons toward the solid surface, whereas the co-axial string of rods features an antiparallel POP-to-OPE $p_1 \rightarrow p_2$ gradient that directs holes away from the solid surface (Fig. 4a). Moreover, hole injection into the p-channel is favourable at any place in the system, that is $n_1 \rightarrow p_2$ in the red domain and $n_2 \rightarrow p_1$ in the yellow domain. The envisioned design fulfils the requirements for the construction of a [2 + 2] OMARG-SHJ.

The donor–acceptor hybrids **1–5** have been prepared by multistep organic synthesis.[8,9] The reactions used involve modern methodology, with repetitive Suzuki and Sonogashira couplings as key steps in the synthesis of the POP and OPE scaffolds, respectively. Detailed descriptions of this substantial synthetic effort can be found elsewhere.[9]

To build oriented and ordered OMARG-SHJs on solid substrates, zipper assembly has been introduced recently (Fig. 3a).[9] In brief, the strained disulfide tail of initiator **1** is used for covalent attachment to gold surfaces. To Au-**1**- monolayers, propagator **2** is added. Intercalation of the lower half of the NDIs of **2** and the NDIs of **1** yields the desired π-stacks. Molecular models confirm that this π-stacking is directed by intrastack hydrogen bonding and interstack ion pairing. The upper half of the NDIs of **2** stays free on the surface of bilayer Au-**1**-**2**-. These cationic sticky ends then are used to zip up with the propagator **3**, which in turn produces anionic sticky ends to zip with **2**, and so on and so forth. At any point during this process, the yellow domain Au-**1**-(**2**-**3**-)$_m$ can be covered with a red domain to give Au-**1**-(**2**-**3**-)$_m$-(**4**-**5**-)$_n$.

Zipper assembly is expected to afford n-type NDI π-stacks aligned along strings of p-type rods (Fig. 3a). These expectations have been supported by molecular models and extensive experimental data on gradient-free zippers. Without going into details, zipper architectures were found to have smoother surfaces, better critical thickness and higher photocurrents than the corresponding layer-by-layer controls, and they respond positively to functional probes such as capping.[9] The critical thickness L_C refers to the thickness where the zipper architecture stops producing more photocurrent. The critical thickness is particularly informative because quartz-crystal microbalance (QCM) controls have shown that photocurrent saturation doesn't occur because the architectures stop growing but because the charges start to recombine within the larger systems before they reach the surfaces and can be used. The best critical thicknesses obtained by zipper assembly of cascade-free SHJs were $L_C \sim 20$ layers.[9]

Experimental conditions

OMARG-SHJs were characterized under routine conditions. For photocurrent generation, the coated gold electrodes obtained by zipper assembly were used as working electrodes. A Pt wire was used as counter electrode and Ag/AgCl as reference electrode. Triethanolamine (TEOA, 50 mM) was used as mobile hole acceptor in deaerated aqueous Na_2SO_4 (100 mM). TEOA as mobile hole acceptor is further important for the photosystem to define the directionality of operational OMARG-SHJs (p_M, Fig. 4). Photocurrents I generated by irradiation with 150 W solar simulator (66 mW cm^{-2}) were measured at +0.4 V *vs.* Ag/AgCl and converted into photocurrent density ($a \sim 0.7$ cm^2).[8]

Typical conditions for zipper assembly were 5–10 μM propagator in 50% aqueous TFE with 0.5 mM sodium phosphate (pH 7) and 100 mM NaCl, two days, room temperature. Zipper assembly of OMARG-SHJs and controls was followed by photocurrent generation and QCM analysis to determine the corresponding mass deposited per layer.[8]

[2 + 2] OMARG-SHJs: Photoinduced charge separation over very long distances

During the assembly of the yellow domain Au-**1**-(**2**-**3**-)$_m$-, the photocurrent density J increased linearly with the number of layers added (Fig. 4b●, layers 2–10). With the addition of the red domain Au-**1**-(**2**-**3**-)$_4$-**2**-(**5**-**4**-)$_n$-, a sharp increase in photocurrent generation was observed (Fig. 4b●, layers 11–16). This change in photocurrent generation reflects the intrinsic activities of the individual domains and has nothing to do with the gradients applied. The intrinsically different activity of yellow and red domains also illustrate nicely that absolute photocurrents values are irrelevant in the current context.

Continuing growth of the red domain in Au-**1**-(**2**-**3**-)$_4$-**2**-(**5**-**4**-)$_m$- continued to generate photocurrent up to ~50 layers in total. The absence of photocurrent saturation with [2 + 2] OMARG-SHJs was in clear contrast to gradient-free architectures with a critical thickness of maximal $L_C \leq 20$ layers. QCM controls confirmed that the gradual onset of photocurrent saturation in Au-**1**-(**2**-**3**-)$_4$-**2**-(**5**-**4**-)$_n$- at 40 layers does not originate from reduced growth. Transmittance simulation suggested that decreasing photocurrents at $L_C > 40$ occurs simply because most of the photons are consumed at this point. This observation suggested that the onset of charge recombination in [2 + 2] OMARG-SHJs Au-**1**-(**2**-**3**-)$_4$-**2**-(**5**-**4**-)$_m$- is not detectable. Under the present conditions, antiparallel two-component gradients in n- and p-channel of OMARG-SHJs thus appear to suffice to achieve photoinduced charge separation over formally "infinite" distances.

The validity of this interpretation was supported by a series of control experiments.[8] Increasing thickness of the yellow domain, for example, reduces the critical thickness of [2 + 2] OMARG-SHJs. This finding is a meaningful indication for the onset of charge recombination within yellow domains of excessive thickness. Most important was the finding that removal of the gradient in the p-channel reduces the critical thickness back to $L_C = 18$ layers (Fig. 4c●). For this control experiment with [2 + 1] "OMARG-SHJs," red propagators with POP in place of the OPE scaffolds in **4** and **5** were synthesized.[9] The J–L profile of [2 + 1] "OMARG-SHJs" showed the same increase in photocurrent when moving from yellow to red domains because of intrinsic differences in activity of the domains and not because of the multicomponent architecture. However, at 20 layers, the photocurrent generated by single-gradient [2 + 1] "OMARG-SHJs" started to decrease. QCM controls confirmed that this decrease originated from the onset of charge recombination in the thicker architectures. The conclusion that both gradients are needed for photoinduced charge separation over very long distance is meaningful. Without antiparallel gradient in the p-channel, directional transport achieved by the gradient in the n-channel NDI stack is useless because the hole can simply follow by free diffusion and recombine anywhere.

[2 + 2] Anti-OMARG-SHJs: Photocurrent inhibition

The inversion of both gradients in OMARG-SHJs Au-**1**-(**2**-**3**-)$_4$-**2**-(**5**-**4**-)$_m$- produces anti-OMARG-SHJs Au-**1′**-(**4**-**5**-)$_4$-**4**-(**3**-**2**-)$_m$-, where holes and electrons are driven in the wrong direction (Fig. 4b). This macroscopic directionality is imposed by the mobile TEOA charge carrier, which accepts holes only and rejects electrons (p_M in Fig. 4). In the J–L profile, the unfavourable [2 + 2] anti-OMARG-SHJs produced initially much more photocurrent than the favourable [2 + 2] OMARG-SHJs (Fig. 4b○). This high activity is observed because the assembly of [2 + 2] anti-OMARG-SHJs begins with the more active red domain Au-**1′**-(**4**-**5**-)$_m$, whereas the assembly of [2 + 2] OMARG-SHJs begins with the less active yellow domain Au-**1**-(**2**-**3**-)$_m$. These differences have nothing to do with the application of redox gradients.

Application of the yellow domain of [2 + 2] anti-OMARG-SHJs Au-**1′**-(**4**-**5**-)$_4$-**4**-(**3**-**2**-)$_n$- caused a clear decrease in photocurrent down to constant residual current

(Fig. 4b○). The same partial photocurrent inhibition was not observed with single-gradient [2 + 1] anti-"OMARG-SHJs" (Fig. 4c○). This difference confirmed that gradients in both the n- and p-channel are needed for photocurrent inhibition.

We were puzzled by the question why photocurrent inhibition in [2 + 2] anti-OMARG-SHJs Au-**1**′-(**4**-**5**-)$_4$-**4**-(**3**-**2**-)$_n$- was incomplete (Fig. 5). The independence of the residual current on zipper thickness suggested that the limiting event occurs at the interface between red and yellow domain. Uphill charge transport suggested that more than one photon should be consumed. The following cycle offers a conceivable explanation (Fig. 5).

Arbitrarily chosen as a beginning, excitation in the red domain (Fig. 5a) could be followed by electron transfer to the gold electrode. The hole left behind can be transferred to the OPE acceptor but not to the mobile carrier because of the interfering POP barrier (Fig. 5b). To reduce the resulting OPE radical cation, excitation in the yellow domain is the only solution (Fig. 5c). The resulting hole can be transferred to the mobile carrier, whereas the movement of the electron to the gold electrode is blocked by the red NDI barrier (Fig. 5d). The resulting yellow NDI radical anion can then recombine with the POP radical cation at the interface between yellow and red domain of the [2 + 2] anti-OMARG-SHJ (Fig. 5e).

This explanation is consistent with the independence of photocurrent inhibition on the thickness of the red domain (Fig. 4b○) as well as the inability of the single-gradient [2 + 1] anti-OMARG-SHJ to inhibit photocurrent generation (Fig. 4c○). This explanation further implies that complete photocurrent inhibition should be achieved with [3 + 3] and higher anti-OMARG-SHJs.

Lateral self-sorting as emerging challenge

The results with a minimalist OMARG-SHJ model summarized in the preceding sections encourage further studies on the topic. However, whereas zipper assembly

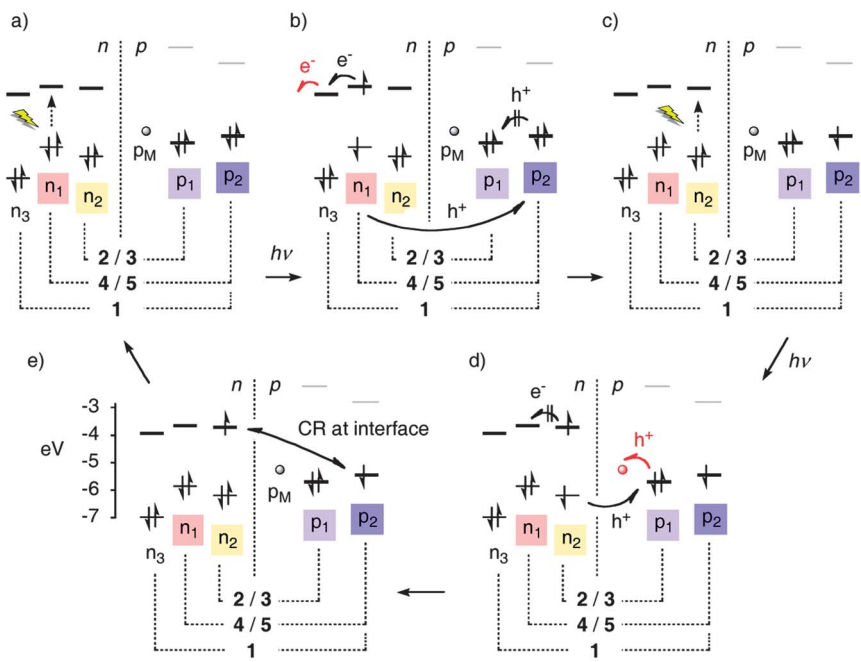

Fig. 5 Why is photocurrent inhibition by [2 + 2] anti-OMARG-SHJs in Fig. 4b○ only partial and thickness independent? A possible explanation.

is a wonderful method to enjoy the power of organic multistep synthesis, it is too demanding for the routine production of OMARG-SHJs. Zipper assembly has been successful to build oriented and ordered surface architectures because unresolved problems in supramolecular chemistry have been bypassed with additional efforts in covalent organic synthesis. More user-friendly low-cost high-speed alternatives to zipper assembly will necessarily have to face these difficulties. With increasing multicomponent complexity as consequence of decreasing covalent input, the question of self-sorting will be of central importance. For 3D architectures built on 2D platforms, lateral self-sorting emerges as a particularly urgent, intimidating but also very stimulating topic. It deserves a thorough discussion.

Self-sorting as such can be defined as molecular assembly where different molecules distinguish between self and non-self.[10] Self-sorting of clearly different molecules is ubiquitous both on the macroscopic and on the molecular level. For instance, (complementary) oligonucleotides and (anionic) phospholipids do not mix randomly and "self-sort" into double stranded helices and bilayer membranes instead. The crystallization of racemates into mixtures of enantiopure crystals is as well appreciated as the phase separation of oil and water. Self-sorting on the molecular level requires the occurrence of molecular recognition and directionality. It becomes really interesting only when very similar, miscible and, at best, mutually attractive components are concerned. Self-sorting has received increasing recent attention with regard to systems such as chemoorthogonal host–guest complexes, capsules, pseudo-rotaxanes, copolymers, fibers, micelles or gels.[10]

Systematic studies on directional self-sorting in 3D surface architectures are rare, conceptual guidelines under-recognized. A brief analysis of the situation reveals the following. In its simplest expression, self-sorting on surfaces concerns the assembly of two components into mixed architectures. In the absence of self-sorting, the two components mix randomly. This random mixing is entropically favored. Self-sorting can be alternate or uniform (Fig. 6). Uniform self-sorting has also been referred to as narcissistic, whereas alternate self-sorting has been referred to as social.[10] In alternate self-sorting, molecules "n" (for negative, including electron transporting) and "p" (for positive, *e.g.*, hole transporting) arrange in a strictly alternate order, every molecule n is surrounded by molecules p, and *vice versa* (Fig. 6a). In uniform self-sorting, molecules n assemble together, usually into large macrodomains, sometimes also into smaller, more demanding but also more interesting "nanodomains" near the molecular level (Fig. 6e and 6f). Usually, macrodomains composed of molecules n do not interact much with the adjacent complementary domains containing molecules p only. Their activities are thus additive but not more, they do not work together.

The combination of alternate and uniform self-sorting on surfaces or, more generally, at interfaces leads to the most challenging and scientifically most attractive and relevant situations. To characterize these systems, self-sorting in the direction parallel to the main compartmentalizing platform of the system is referred to as lateral. This can be a solid surface, the surface of a lipid bilayer membrane, and so on. The complementary direction is referred as axial and, for simplicity only, assumed to be perpendicular to the compartmentalizing platform of the system. Examples include the long axis of DNA duplex or other π-stacks, an α-helix, and so on.

From this point of view, purely alternate self-sorting is defined as both alternate axial (AA) and alternate lateral self-sorting (AL, Fig. 6a). Transition to uniform lateral self-sorting (UL) with preserved AA organization leads to the UL-AA situation that is of interest with lipid bilayer membranes (Fig. 6b).[11] The complementary transition to uniform axial self-sorting (UA) with preserved AL yields the AL-UA systems needed for the construction of SHJ photosystems (Fig. 6c, 6d).[4,7,8]

AL-UA self-sorting with two similar components n_1 and n_2 against two similar components p_1 and p_2 can occur in a parallel (P) or in an antiparallel manner (A). In AL-UAP systems, alternate lateral self-sorting of components n_1 and p_1 followed

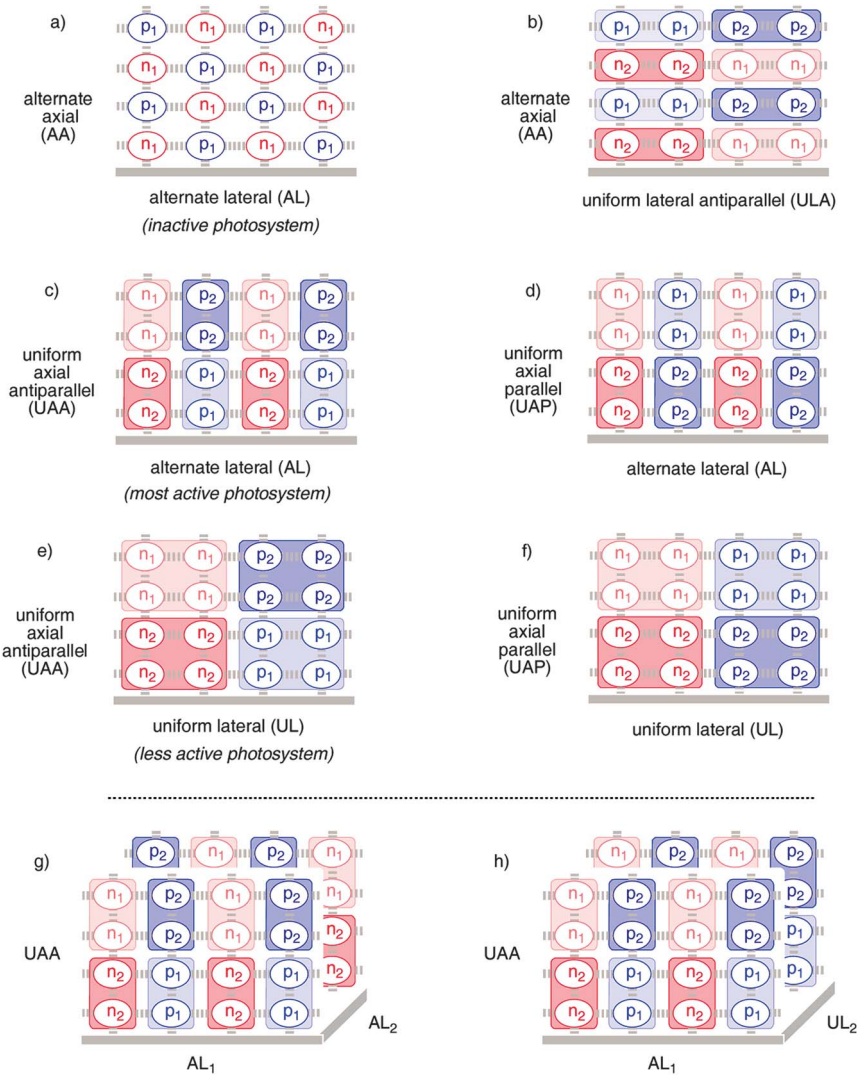

Fig. 6 Self-sorting of molecules n and p into representative architectures of scientific relevance. For artificial photosynthesis, OMARG-SHJs should be best (c, e), macrodomains should be less active (e) and alternate systems should be inactive (a). The proposed terminology is new and subject to discussion.

alternate lateral self-sorting of components n_2 and p_2 generates $1 \rightarrow 2$ gradients in n and p channels that are oriented in a parallel manner (Fig. 6d). This architecture is incompatible with OMARG-SHJs (it's actually an anti-OMARG-SHJ, see Fig. 4). In the complementary AL-UAA systems, antiparallel $1 \rightarrow 2$ gradients in n and p channels are obtained (Fig. 6c). This is the architecture of OMARG-SHJs.[7,8]

Transition from alternate to uniform lateral self-sorting in AL-UA systems produces formal UL-UA macrodomains, which again can contain parallel (UL-UAP, Fig. 6f) or antiparallel gradients in axial direction (UL-UAA, Fig. 6e). In artifical photosystems, UL-UA macrodomains with reduced n/p-interface should have reduced activity (Fig. 1a). General strategies to control the transition from the less active UL-UA macrodomains (UL-UA, Fig. 6e) to the more active OMARG-SHJs (AL-UA, Fig. 6c) remain to be discovered.

So far, the definition of self-sorting ignores the third dimension. For the ideal AL-UAA system, for example, the adjacent layer in the third dimension can in principle be added either in alternate (Fig. 6g) or in uniform mode (Fig. 6h). However, it seems safe to assume that lateral self-sorting is identical in all directions (Fig. 6g).

These conceptual considerations on self-sorting cover just a few relevant cases in a highly simplified manner. A more systematic treatment will reveal many more possibilities with rapidly increasing complexity. However, inspection of leading recent examples suggests that self-sorting has the potential to become a surprisingly powerful and promising method to build functional supramolecular architectures.

Recent examples for self-sorting

Charge-transfer or aromatic electron donor–acceptor complexes between π-basic and π-acidic aromatics are the classical example for alternate self-sorting in π-stack architectures (Fig. 6a).[12] For instance, according to the deep red color of their charge-transfer complexes, all mixtures of π-acidic NDIs **6** and π-basic dialkoxy-naphthyls (DANs) **7** exhibit alternate self-sorting in liquid-crystalline phase at elevated temperature (except for mixtures with the racemic **6E**, which does not form liquid crystals, Fig. 7).

Upon cooling and transition from the liquid-crystalline mesophase to the crystalline phase, the red color indicative for alternate self-sorting is preserved for mixtures of α-branched NDIs **6D** and **6E** with DANs **7A–7H** without α-branched tails (Fig. 7, black squares). NDIs **6A–6C** without α-branching do not form co-crystals (Fig. 7, white squares) or give co-crystals that rapidly loose their red color (Fig. 7, light squares). This thermochromism was interpreted as transition from alternate to axial uniform self-sorting upon phase transition from liquid-crystalline to crystalline phase (Fig. 7, light squares). Co-crystals of NDI **6B** and DANs **7D–7H** with tails of similar length preserve some pink color. According to data from X-ray diffraction and absorption spectroscopy, this pink color indicates a partial preservation of alternate self-sorting in the solid state. Self-sorting of the molecules in co-crystals with α-branching for both NDI **6D** and DANs **7I** and **7J** changed to uniform in the solid state.

Taken together, these findings implied that α-branching on the NDI side serves as steric barrier to stabilize the alternate π-stacks, whereas additional α-branching on the DAN side destabilizes the alternate π-stacks. Moreover, topologically matched tails favor alternate self-sorting (Fig. 6a), whereas topologically mismatched tails favor uniform self-sorting into macrodomains (Fig. 6e, f). Finally, enantiopurity matters; racemic mixtures give different and less reliable results.

Self-sorting upon co-assembly of the same partners has been studied in methylcyclohexane/chloroform 95 : 5 (Fig. 7).[13] According to the charge-transfer band at 550 nm, co-assembly of π-acid **6F** and π-base **7 K** exhibits uniform self-sorting in purest form with linear behavior over the full mole fraction range. In clear contrast, π-acid **6G** and π-base **7 K** afford alternate self-sorting. This finding is meaningful because in **6G** and **7 K**, the positions of the hydrazide and amide H-bond donors and acceptors match to form H-bonded chains along the alternately self-sorted π-stacks, whereas in **6F** and **7 K**, the positions of H-bond donors and acceptors are mismatched and can form H-bonded chains only along uniformly but not alternately self-sorted π-stacks.

In methylcyclohexane/chloroform 8 : 2, perylenediimide (PDI) **8A** self-assembles into H-aggregates (Fig. 8).[14] Steric interference from γ-branching causes PDI **8B** to self-assemble into the more twisted, less favorable J-aggregates. Co-assembly of PDIs **8A** with **8B** yields H-aggregates until a roughly stoichiometric amount of **8B** is added. This implies that PDI **8B** can be incorporated into H-aggregates of PDI **8A** until alternate self-sorting is reached around a mole fraction $x \sim 0.5$. Even at $x > 0.5$, the same H-aggregates of **8A** and **8B** would form preferentially with the excess **8B** forming J-aggregates. This transition produces a non-linear x-profile with biphasic behavior for the spectroscopic signatures of H- and J-aggregates.

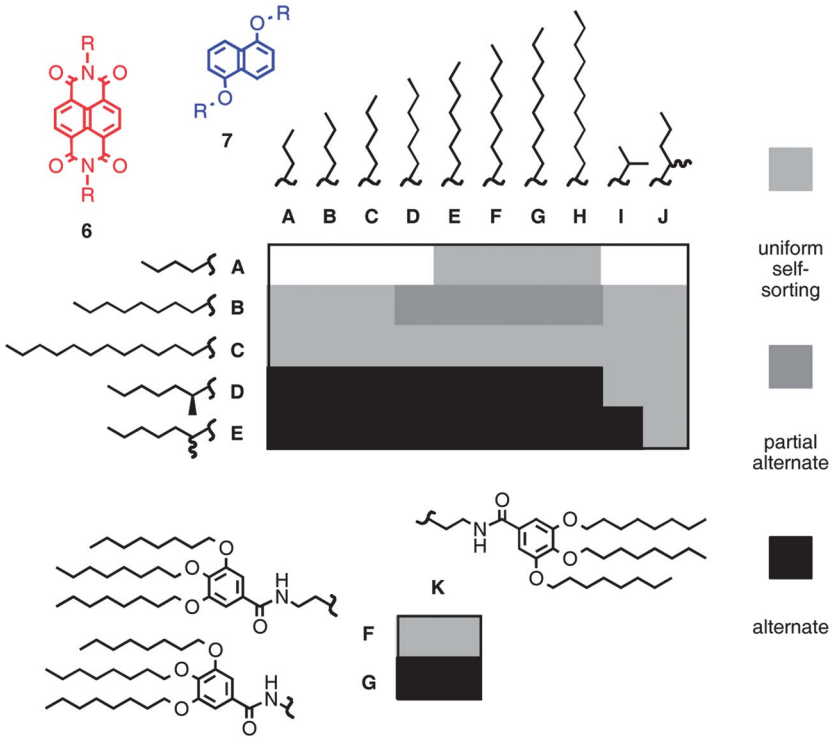

Fig. 7 Alternate and uniform self-sorting by cooling from alternately self-sorted liquid-crystalline phases of π-acids **6A–6E** and π-bases **7A–7J** (top, white squares: no co-crystals) and by self-assembly of **6F–6G** and **7 K** in solution.

The twist angle of aromatic planes offers one of the most sophisticated origins for the self-sorting of π-stacks.[15] PDIs **9A–9D** with different twist angle caused by substituents in their core have been found to undergo uniform axial self-sorting when forming π-stacks in solution. Results from covalent capture of cyclic dimers by disulfide formation support insights from aggregation studies. At high enough concentrations, mainly homodimers such as $\mathbf{9A_2}$ or $\mathbf{9D_2}$ but no heterodimers such as **9AD** are observed. *En route* to π-stacks, homodimers could further dimerize into co-catenated homotetramers, and self-sorting of the chiral PDIs **9D** was stereoselective. Intramolecular disulfide formation occurs at high dilution. Random mixing of planar PDIs **9A** and **10** confirmed the twist angle of the aromatic planes as origin of uniform self-sorting.

Many more studies that include self-sorting in one way or the other have appeared in the recent literature, including organic solar cells with efficiencies up to 2.5%.[4] However, this brief inspection of the few most pertinent examples already illustrates nicely that uniform axial self-sorting of π-stacks is often preferred over random or alternate self-sorting driven by aromatic donor–acceptor interactions. Moreover, subtle structural differences can influence self-sorting in a significant and rational manner. These results encourage ongoing efforts to use self-sorting for the creation of ordered and oriented functional surface architectures such as OMARG-SHJs.[16]

Summary and outlook

The objective of this discussion was to put the concept of OMARG-SHJ photosystems on the table and elaborate on self-sorting strategies as practical method to get

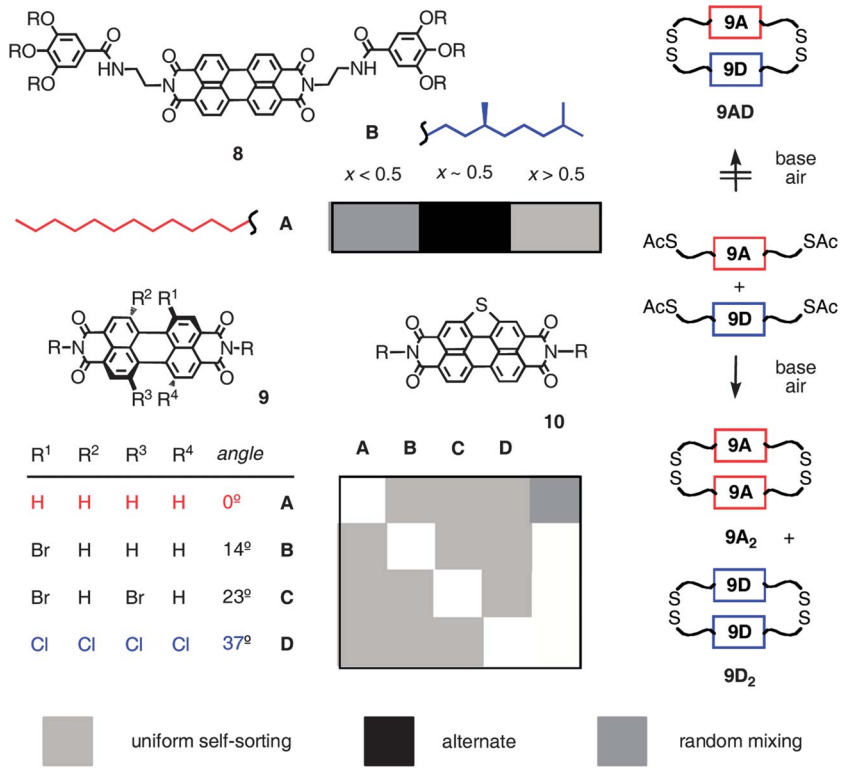

Fig. 8 Axial self-sorting in solution for PDI stacks with different sidechains (**8A–8B**) or different twist angles of their aromatic planes (**9A–9D**, **10**).

there. Probing lessons from nature, OMARG-SHJs consist of molecular hole- and electron-transporting channels that are equipped with oriented antiparallel redox gradients (Fig. 2). Preliminary results suggest that minimalist OMARG-SHJs with two-component gradients in both n- and p-channels already suffice to achieve photoinduced charge separation over very long distances, that both gradients are essential for this purpose, and that the inversion of both gradients causes photocurrent inhibition (Fig. 4). Whereas these results appear interesting enough to justify further studies on ordered and oriented functional multicomponent architectures, the current approach with zipper assembly requires too much covalent organic synthesis to be used routinely and applied broadly. Any reduction of covalent preorganization to minimize synthetic efforts, however, will necessarily increase the importance of self-sorting for the construction of ordered and oriented supramolecular architectures. A few relevant concepts on self-sorting are presented here for discussion. The basic considerations are that axial growth of two-component architectures from surfaces can occur randomly, with alternate self-sorting, or with uniform self-sorting. Uniform axial self-sorting can further occur with uniform or alternate lateral self-sorting (Fig. 6).

A more systematic treatment of self-sorting reveals many more possibilities of rapidly increasing complexity. However, already the current simplistic analysis demonstrates that the identification and characterization of self-sorted systems on the surface will not be easy. Most routine methods for structure determination will fail. However, changes in activity will provide a valuable functional readout for self-sorting in artificial photosystems. The rules appear simple: 1) Alternate lateral and uniform antiparallel axial (AL-UAA) self-sorting into OMARG-SHJs

architectures will give highest activities (Fig. 6c). 2) At constant uniform axial self-sorting, the transition to uniform lateral self-sorting into bilayer-type macrodomains will reduce activity (Fig. 6e), whereas 3) alternate lateral and axial self-sorting will afford inactive photosystems because the charges cannot move (Fig. 6a). Ongoing studies in this direction invite for highest expectations and will be reported in due course.[16]

Acknowledgements

We thank all past coworkers and past and present collaborators for contributions to this research, and the University of Geneva, the NCCR Chemical Biology and the Swiss NSF for financial support. J. A. acknowledges a Marie Curie Fellowship, E. O. is a Sciex Fellow, S. M. an ERC Advanced Investigator.

References

1 (*a*) A. C. Benniston and A. Harriman, *Mater. Today*, 2008, **11**, 26–34; (*b*) R. Ziessel and A. Harriman, *Chem. Commun.*, 2011, **47**, 611–631; (*c*) D. Gust, T. A. Moore and A. L. Moore, *Acc. Chem. Res.*, 2001, **34**, 40–48; (*d*) G. D. Scholes and G. Rumbles, *Nat. Mater.*, 2006, **5**, 683–696; (*e*) L. Sun, L. Hammarström, B. Åkermark and S. Styring, *Chem. Soc. Rev.*, 2001, **30**, 36–49; (*f*) A. W. Roszak, T. D. Howard, J. Southall, A. T. Gardiner, C. J. Law, N. W. Isaacs and R. J. Cogdell, *Science*, 2003, **302**, 1969–1972; (*g*) J. Deisenhofer and H. Michel, *Science*, 1989, **245**, 1463–1473; (*h*) N. Nelson and A. Ben-Shem, *Nat. Rev. Mol. Cell Biol.*, 2004, **5**, 971–982; (*i*) S. Bhosale, A. L. Sisson, P. Talukdar, A. Fürstenberg, N. Banerji, E. Vauthey, G. Bollot, J. Mareda, C. Röger, F. Würthner, N. Sakai and S. Matile, *Science*, 2006, **313**, 84–86; (*j*) A. Perez-Velasco, V. Gorteau and S. Matile, *Angew. Chem., Int. Ed.*, 2008, **47**, 921–923.

2 (*a*) M. Granström, K. Petritsch, A. C. Arias, A. Lux, M. R. Andersson and R. H. Friend, *Nature*, 1998, **395**, 257–260; (*b*) C. W. Tang, *Appl. Phys. Lett.*, 1986, **48**, 183–185; (*c*) S. Sista, Y. Yao, Y. Yang, M. L. Tang and Z. Bao, *Appl. Phys. Lett.*, 2007, **91**, 223508–223508; (*d*) H. Sirringhaus, P. J. Brown, R. H. Friend, M. M. Nielsen, K. Bechgaard, B. M. W. Langeveld-Voss, A. J. H. Spiering, R. A. J. Janssen, E. W. Meijer, P. Herwig and D. M. de Leeuw, *Nature*, 1999, **401**, 685–688; (*e*) G. Bottari, G. de la Torre, D. M. Guldi and T. Torres, *Chem. Rev.*, 2010, **110**, 6768–6816; (*f*) Y. Kim, S. Cook, S. M. Tuladhar, S. A. Choulis, J. Nelson, J. R. Durrant, D. D. C. Bradley, M. Giles, I. McCulloch, C.-S. Ha and M. Ree, *Nat. Mater.*, 2006, **5**, 197–203; (*g*) J. L. Segura, N. Martín and D. M. Guldi, *Chem. Soc. Rev.*, 2005, **34**, 31–47; (*h*) J. Y. Kim, K. Lee, N. E. Coates, D. Moses, T.-Q. Nguyen, M. Dante and A. J. Heeger, *Science*, 2007, **317**, 222–225; (*i*) B. C. Thompson and J. M. J. Fréchet, *Angew. Chem., Int. Ed.*, 2008, **47**, 58–77; (*j*) S. Gnes, H. Neugebauer and N. S. Sariciftci, *Chem. Rev.*, 2007, **107**, 1324–1338; (*k*) C. Ma, M. Fonrodona, M. C. Schikora, M. M. Wienk, R. A. J. Janssen and P. Bäuerle, *Adv. Funct. Mater.*, 2008, **18**, 3323–3331; (*l*) J.-F. Eckert, J.-F. Nicoud, J.-F. Nierengarten, S.-G. Liu, L. Echegoyen, N. Armaroli, F. Barigelletti, L. Ouali, V. Krasnikov and G. Hadziioannou, *J. Am. Chem. Soc.*, 2000, **122**, 7467–7479; (*m*) V. Balzani, M. Venturi and A. Credi, *Molecular Devices and Machines*, Wiley-VCH, Weinheim, 2003; (*n*) F. Yang, M. Shtein and S. Forrest, *Nat. Mater.*, 2004, **4**, 37–41; (*o*) S. Fukuzumi, *Bull. Chem. Soc. Jpn.*, 2006, **79**, 177–195; (*p*) J. Roncali, *Acc. Chem. Res.*, 2009, **42**, 1719–1730.

3 (*a*) B. Oregan and M. Grätzel, *Nature*, 1991, **353**, 737–740; (*b*) J.-H. Yum, D. Hagberg, S.-J. Moon, K. M. Karlsson, T. Marinado, L. Sun, A. Hagfeldt, M. K. Nazeeruddin and M. Grätzel, *Angew. Chem., Int. Ed.*, 2008, **48**, 1576–1580; (*c*) T. Daeneke1, T.-H. Kwon, A. B. Holmes, N. W. Duffy, U. Bach and L. Spiccia, *Nat. Chem.*, 2011, **3**, 211–215.

4 (*a*) F. Würthner and K. Meerholz, *Chem.–Eur. J.*, 2010, **16**, 9366–9373; (*b*) D. M. Bassani, L. Jonusauskaite, A. Lavie-Cambot, N. D. McClenaghan, J.-L. Pozzo, D. Ray and G. Vives, *Coord. Chem. Rev.*, 2010, **254**, 2429–2445; (*c*) M. R. Wasielewski, *Acc. Chem. Res.*, 2009, **42**, 1910–1921; (*d*) W. Li, A. Saeki, Y. Yamamoto, T. Fukushima, S. Seki, N. Ishii, K. Kato, M. Takata and T. Aida, *Chem.–Asian J.*, 2010, **5**, 1566–1572; (*e*) Y. Hizume, K. Tashiro, R. Charvet, Y. Yamamoto, A. Saeki, S. Seki and T. Aida, *J. Am. Chem. Soc.*, 2010, **132**, 6628–6629; (*f*) L. Bu, X. Guo, B. Yu, Y. Qu, Z. Xie, D. Yan, Y. Geng and F. Wang, *J. Am. Chem. Soc.*, 2009, **131**, 13242–13243; (*g*) A. Kira, T. Umeyama, Y. Matano, K. Yoshida, S. Isoda, J. K. Park, D. Kim and H. Imahori, *J. Am. Chem. Soc.*, 2009, **131**, 3198–3200; (*h*) K. Sugiyasu, S. Kawano, N. Fujita and

S. Shinkai, *Chem. Mater.*, 2008, **20**, 2863–2865; (*i*) P. Jonkheijm, N. Stutzmann, Z. Chen, D. M. de Leeuw, E. W. Meijer, A. P. H. J. Schenning and F. Würthner, *J. Am. Chem. Soc.*, 2006, **128**, 9535–9540; (*j*) Y. Yamamoto, T. Fukushima, Y. Suna, N. Ishii, A. Saeki, S. Seki, S. Tagawa, M. Taniguchi, T. Kawai and T. Aida, *Science*, 2006, **314**, 1761–1764; (*k*) C. Ehli, C. Oelsner, D. M. Guldi, A. Mateo-Alonso, M. Prato, C. Schmidt, C. Backes, F. Hauke and A. Hirsch, *Nat. Chem.*, 2009, **1**, 243–249.

5 (*a*) D. M. Kaschak, J. T. Lean, C. C. Waraksa, G. B. Saupe, H. Usami and T. E. Mallouk, *J. Am. Chem. Soc.*, 1999, **121**, 3435–3445; (*b*) G. Decher, *Science*, 1997, **277**, 1232–1237; (*c*) D. M. Guldi, G. M. A. Rahman, M. Prato, N. Jux, S. Qin and W. Ford, *Angew. Chem., Int. Ed.*, 2005, **44**, 2015–2018; (*d*) J. K. Mwaura, M. R. Pinto, D. Witker, N. Ananthakrishnan, K. S. Schanze and J. R. Reynolds, *Langmuir*, 2005, **21**, 10119–10126; (*e*) A. B. F. Martinson, A. M. Massari, S. J. Lee, R. W. Gurney, K. E. Splan, J. T. Hupp and S. T. Nguyen, *J. Electrochem. Soc.*, 2006, **153**, A527–A532; (*f*) A. Kira, T. Umeyama, Y. Matano, K. Yoshida, S. Isoda, J. K. Park, D. Kim and H. Imahori, *J. Am. Chem. Soc.*, 2009, **131**, 3198–3200; (*g*) D. M. Guldi, I. Zilbermann, G. Anderson, A. Li, D. Balbinot, N. Jux, M. Hatzimarinaki, A. Hirsch and M. Prato, *Chem. Commun.*, 2004, 726–727; (*h*) F. B. Abdelrazzaq, R. C. Kwong and M. E. Thompson, *J. Am. Chem. Soc.*, 2002, **124**, 4796–4803; (*i*) M. Morisue, S. Yamatsu, N. Haruta and Y. Kobuke, *Chem.–Eur. J.*, 2005, **11**, 5563–5574.

6 (*a*) H. J. Snaith, G. L. Whiting, B. Sun, N. C. Greenham, W. T. S. Huck and R. H. Friend, *Nano Lett.*, 2005, **5**, 1653–1657; (*b*) R. C. Shallcross, G. D. D'Ambruoso, B. D. Korth, H. K. Hall, Z. Zheng, J. Pyun and N. R. Armstrong, *J. Am. Chem. Soc.*, 2007, **129**, 11310–11311; (*c*) E. Hwang, K. M. N. de Silva, C. B. Seevers, J.-R. Li, J. C. Garno and E. E. Nesterov, *Langmuir*, 2008, **24**, 9700–9706; (*d*) S. Foster, C. E. Finlayson, P. E. Keivanidis, Y.-S. Huang, I. Hwang, R. H. Friend, M. B. J. Otten, L.-P. Lu, E. Schwartz, R. J. M. Nolte and A. E. Rowan, *Macromolecules*, 2009, **42**, 2023–2030.

7 R. Bhosale, J. Misek, N. Sakai and S. Matile, *Chem. Soc. Rev.*, 2010, **39**, 138–149.

8 N. Sakai, R. Bhosale, D. Emery, J. Mareda and S. Matile, *J. Am. Chem. Soc.*, 2010, **132**, 6923–6925.

9 (*a*) N. Sakai, A. L. Sisson, T. Bürgi and S. Matile, *J. Am. Chem. Soc.*, 2007, **129**, 15758–15759; (*b*) A. L. Sisson, N. Sakai, N. Banerji, A. Fürstenberg, E. Vauthey and S. Matile, *Angew. Chem., Int. Ed.*, 2008, **47**, 3727–3729; (*c*) R. S. K. Kishore, O. Kel, N. Banerji, D. Emery, G. Bollot, J. Mareda, A. Gomez-Casado, P. Jonkheijm, J. Huskens, P. Maroni, M. Borkovec, E. Vauthey, N. Sakai and S. Matile, *J. Am. Chem. Soc.*, 2009, **131**, 11106–11116; (*d*) R. Bhosale, A. Perez-Velasco, V. Ravikumar, R. S. K. Kishore, O. Kel, A. Gomez-Casado, P. Jonkheijm, J. Huskens, P. Maroni, M. Borkovec, T. Sawada, E. Vauthey, N. Sakai and S. Matile, *Angew. Chem., Int. Ed.*, 2009, **48**, 6461–6464.

10 (*a*) A. X. Wu and L. Isaacs, *J. Am. Chem. Soc.*, 2003, **125**, 4831–4835; (*b*) N. A. Schnarr and A. J. Kennan, *J. Am. Chem. Soc.*, 2003, **125**, 6364–6365; (*c*) M. de Loos, A. Friggeri, J. van Esch, R. M. Kellogg and B. L. Feringa, *Org. Biomol. Chem.*, 2005, **3**, 1631–1639; (*d*) W. Jiang and C. A. Schalley, *Proc. Natl. Acad. Sci. U. S. A.*, 2009, **106**, 10425–10429; (*e*) D. Ajami, J.-L. Hou, T. J. Dale, E. Barrett and J. Rebek Jr, *Proc. Natl. Acad. Sci. U. S. A.*, 2009, **106**, 10430–10434; (*f*) N. Tomimasu, A. Kanaya, Y. Takashima, H. Yamaguchi and A. Harada, *J. Am. Chem. Soc.*, 2009, **131**, 12339–12343; (*g*) N. E. Botterhuis, S. Karthikeyan, A. J. H. Spiering and R. P. Sijbesma, *Macromolecules*, 2010, **43**, 745–751.

11 (*a*) O. A. Kucherak, S. Oncul, Z. Darwich, D. A. Yushchenko, Y. Arntz, P. Didier, Y. Mély and A. S. Klymchenko, *J. Am. Chem. Soc.*, 2010, **132**, 4907–4916; (*b*) T. Baumgart, G. Hunt, E. R. Farkas, W. W. Webb and G. W. Feigenson, *Biochim. Biophys. Acta*, 2007, **1768**, 2182–2194; (*c*) S. D. Connell and D. A. Smith, *Mol. Membr. Biol.*, 2006, **23**, 17–28; (*d*) J. Zhang, B. Jing, N. Tokutake and S. L. Regen, *Biochemistry*, 2005, **44**, 3598–3603.

12 P. M. Alvey, J. J. Reczek, V. Lynch and B. L. Iverson, *J. Org. Chem.*, 2010, **75**, 7682–7690.

13 M. R. Molla, A. Das and S. Ghosh, *Chem.–Eur. J.*, 2010, **16**, 10084–10093.

14 S. Ghosh, X.-Q. Li, V. Stepanenko and F. Würthner, *Chem.–Eur. J.*, 2008, **14**, 11343–11357.

15 A. D. Shaller, W. Wang, H. Gan and A. D. Q. Li, *Angew. Chem. Int. Ed.*, 2008, **47**, 7705–7709.

16 M. Lista, N. Sakai, O. Kel, J. Areephong, S. Sakurai, D. Emery, J. Mareda, E. Vauthey and S. Matile, in preparation.